Protein Microdevices

DOI: 10.1002/anie.201105925

Dynamically Tunable Protein Microlenses**

Yun-Lu Sun, Wen-Fei Dong, Rui-Zhu Yang, Xiang Meng, Lu Zhang, Qi-Dai Chen, and Hong-Bo Sun**

Proteins have been utilized in numerous photonic and optoelectronic devices, for example, in optical computation,[1] organic light emitting diodes (OLEDs),[2] waveguides,[3] bio-micro/nanolasers,[3] organic field effect transistors (OFETs),[4] and memory devices, because their unique optical, mechanical, electrical, and chemical properties are easily tailored to each application.[5] The performance of as-prepared protein-based photonic devices has been demonstrated to exceed that of devices that are made with currently available organic materials.[1–12] The underlying motivation for the use of proteins in microdevices is not only abundance, inexpensiveness, and biodegradability, but also biocompatibility and the capacity to tune their properties through appropriate external stimuli. These features are highly desirable for biologically inspired microdevices, for example delicate miniaturized lenses that are similar to the "camera-type" eyes of human beings, the compound eyes of insects, the photosensitive microlens arrays of brittlestars, or the infrared-sensitive microlens receptor arrays of the fire beetle (Melanophila acuminata).[13–15] Scientists have been highly motivated to fabricate these lens-like micro/nanostructures with the aim of producing small, multifunctional, artificial eyes by using dynamically adjustable and fully biocompatible proteins. However, the preparation of protein microlenses that have controlled geometry and precise positioning still poses a challenge.

Herein, we report a promising approach for the production of biomimetic protein microlenses by facile and rapid maskless femtosecond laser direct writing (FsLDW). FsLDW is a well-known method for producing complicated 3D structures with nanometric resolution.[16] Recently, pioneering work from Shear and co-workers demonstrated that protein hydrogel-based microstructures fabricated by FsLDW exhibit a unique responsiveness to chemical signals. This responsiveness could result in rapid and reversible changes in the size and shape of the structures after stimulation by environmental triggers.[17] However, to our knowledge there are few reports on the development of practical and useful devices, such as a tunable microlens, that are made from this class of proteins.

In this study, commercial bovine serum albumin (BSA, 300–500 mg mL^{-1} in aqueous solution) and a photosensitizer (methylene blue, MB, 0.6 mg mL^{-1}) were used to fabricate micro/nanoarchitectures. The cross-linking reaction is initiated through the excitation of photosensitive molecules to their triplet states. The photoexcited molecules then react directly with oxidizable moieties (type I process) or transfer the energy to ground state molecular oxygen (type II process) to form a reactive oxygen species, such as singlet oxygen ($^1O_2$). In either case, excited-state intermediates catalyze the inter or intramolecular covalent cross-linking of oxidizable protein residues (see Scheme S1 in the Supporting Information). In other words, proteins with photooxidizable groups, such as Tyr, Trp, His, Met, and Cys, can absorb infrared or UV light to form reactive or ionized species that are capable of cross-linking with other oxidizable moieties. This mechanism appears to play a role in the formation of some types of cataracts and in the aging of skin.[18–20] BSA and other proteins with oxidizable side chains "inherit" this photo-cross-linking ability, and can thus be used for multiphoton fabrication (Figure 1).

Proof-of-concept protein microlenses were fabricated by using a FsLDW system of our own construction (Figure 1). The system was composed of a femtosecond titanium/sapphire laser (Spectra Physics 3960-X1BB), a piezo stage with a precision of 1 nm (Physik Instrumente P-622.ZCD), and a set of two galvano mirrors. The 3D shapes of the microstructures were designed by using 3Ds Max and then the designs were converted into computer processing programs. Prior to the photo-cross-linking of the proteins at the focal spot, the beam from the femtosecond laser (80 MHz repetition rate, 120 fs pulse width, 780 nm central wavelength) was tightly focused by a high-numerical-aperture (NA = 1.35) oil-immersion objective lens (60×). The horizontal and vertical scanning movements of the focused laser spot were achieved simultaneously by the two-galvano-mirror set and the piezo stage.[21,22] After cross-linking, the sample was rinsed in water several times to remove unreacted proteins. Then the as-formed protein microstructures were left on the chip.

Surface topography (shape and roughness) plays an important role in the optical properties of protein micro-optics. However, the surface roughness of BSA microstruc-

[*] Y. L. Sun, Prof. Dr. W. F. Dong, R. Z. Yang, X. Meng, L. Zhang, Prof. Dr. Q. D. Chen, Prof. Dr. H. B. Sun
State Key Laboratory on Integrated Optoelectronics
College of Electronic Science and Engineering
Jilin University, 2699 Qianjin Street
Changchun 130012 (China)
E-mail: dongwf@jlu.edu.cn
hbsun@jlu.edu.cn
Prof. Dr. H. B. Sun
College of Physics, Jilin University
119 Jiefang Road, Changchun 130023 (China)
E-mail: hbsun@jlu.edu.cn

[**] This work was supported by the National Science Foundation of China (Grant Nos. 61137001, 91123029, 90923037, and 61077066) and the National Basic Research Program of China (973 Program) (Grant No. 2011CB013005).

Supporting information for this article is available on the WWW under http://dx.doi.org/10.1002/anie.201105925.

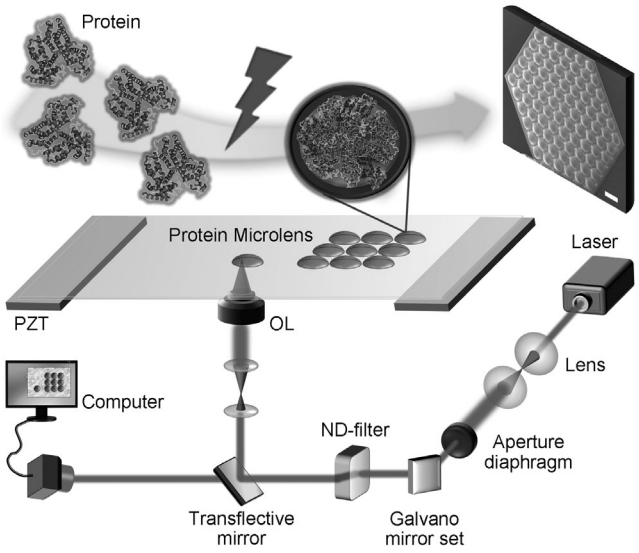

Figure 1. The preparation of protein microarchitectures by maskless, femtosecond laser 3D direct writing (FsLDW). The protein molecules are cross-linked by a two-photon polymerization (TPP) approach to form a hydrogel. The process is then repeated to obtain 3D functional microstructures. As an example, an SEM image of a protein microlens array is shown in the top right corner of the figure. Scale bar: 10 μm.

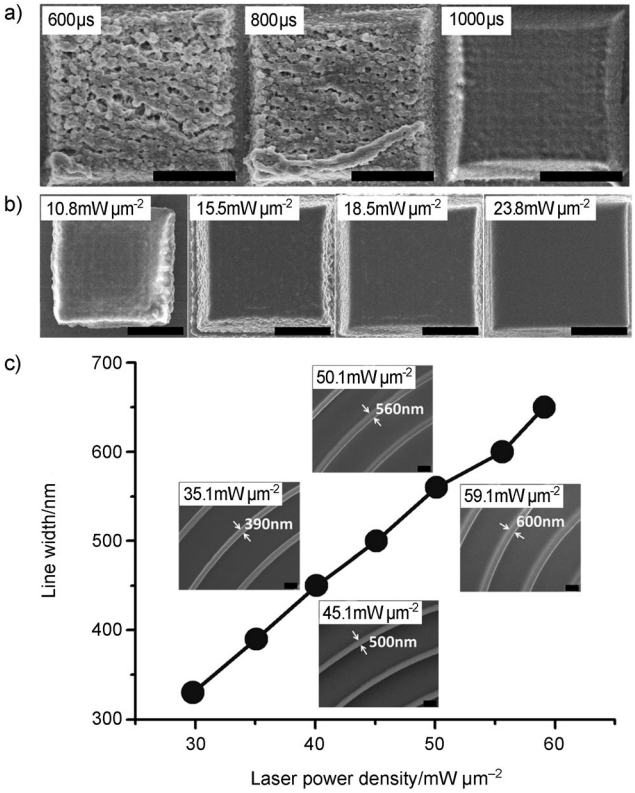

Figure 2. a) Topography of protein microdevices fabricated with different exposure times on a single point (varying inversely with scanning speed). The average laser power density is fixed at approximately 20 mW μm^{-2}. Scale bar: 5 μm. b) Topography of protein microdevices fabricated with different average laser power-densities when exposure time on single point is fixed at 1000 μs. Scale bar: 5 μm. c) Relationship between the line width and laser power density (the laser power was measured in front of the objective). The focal spot area where polymerization occurs is calculated to be approximately 0.40 μm^2, which is used to estimate the mean laser power density in the focus area. Inset: SEM images of lines under different laser power-densities. Scale bar: 1 μm.

tures fabricated by FsLDW is usually too rough (more than 100 nm) to be utilized in optical applications.[17] Therefore, improving the surface appearance of the microdevices was the highest priority in this study. Previously, we found a very interesting self-smoothing behavior of commercial SU-8 resins during FsLDW fabrication: the surface roughness of highly cross-linked SU-8 microstructures decreased after rinsing with a developer.[23,24] It is supposed that this self-smoothing behavior may be directed by local surface tension during the rinsing step. We also found that a sufficiently small scanning step and a high homogeneity of the voxel sizes were the major factors that influence the self-smoothing effect. As the homogeneity of the voxel sizes is related to the quadratic dependence of photopolymerization rate on the laser light intensity, slight variations in pulse energy may induce significant unevenness of the surface. For this reason, the fluctuation of the laser pulse energy has to be designed at lower than 0.5% to achieve the self-smoothing effect. The local temperature around the laser should be maintained within (23 ± 0.2) °C and an output feedback system should be used. Other processing parameters, such as the concentration of protein, the laser power density, the exposure time on a single point, and the scanning step should be carefully optimized to improve the overall surface quality of protein microstructures (Figure 2). A high protein concentration (400–500 mg mL^{-1}) was helpful in obtaining mechanically stable architectures. Furthermore, by properly increasing both the exposure time (from 600 μs to 1000 μs) and the average laser power density (from 10 mW μm^{-2} to 24 mW μm^{-2}), the surface of the as-prepared protein microstructures became smooth enough for optical applications (Figure 2a and Figure 2b). The average surface roughness decreased to approximately 5 nm or even less when the laser power density and exposure time were approximately 24 mW μm^{-2} and 1000 μs, respectively (see Figure S2 in the Supporting Information). Furthermore, the feature sizes of the protein lines were strongly dependent on the laser power density (Figure 2c). The minimum feature size of the line width (about 250 nm with fine topography) was achieved under the following optimized conditions: an exposure time of 1000 μs, laser power density of approximately 20 mW μm^{-2}, and a concentration of BSA of 400 mg mL^{-1}. Under these conditions, arbitrarily designed and precisely positioned microstructures were easily produced (Figure 2, Figure 3, and Figure 4; see also Figure S2 in the Supporting Information). For example, the 3D relief portrait of a face with a size of 40 μm × 30 μm and a height of 15 μm was generated within 30 min (Figure 3).

As photo-cross-linked BSA micro/nanostructures contain weak acidic and weak basic pendant groups, these pH-sensitive groups will become protonated or deprotonated as the pH value varies. Therefore, the electrostatic interaction between these groups can be manipulated. This manipulation results in the swelling or shrinking of the protein micro/nanostructures. As shown in Figure 3a, the face swelled to

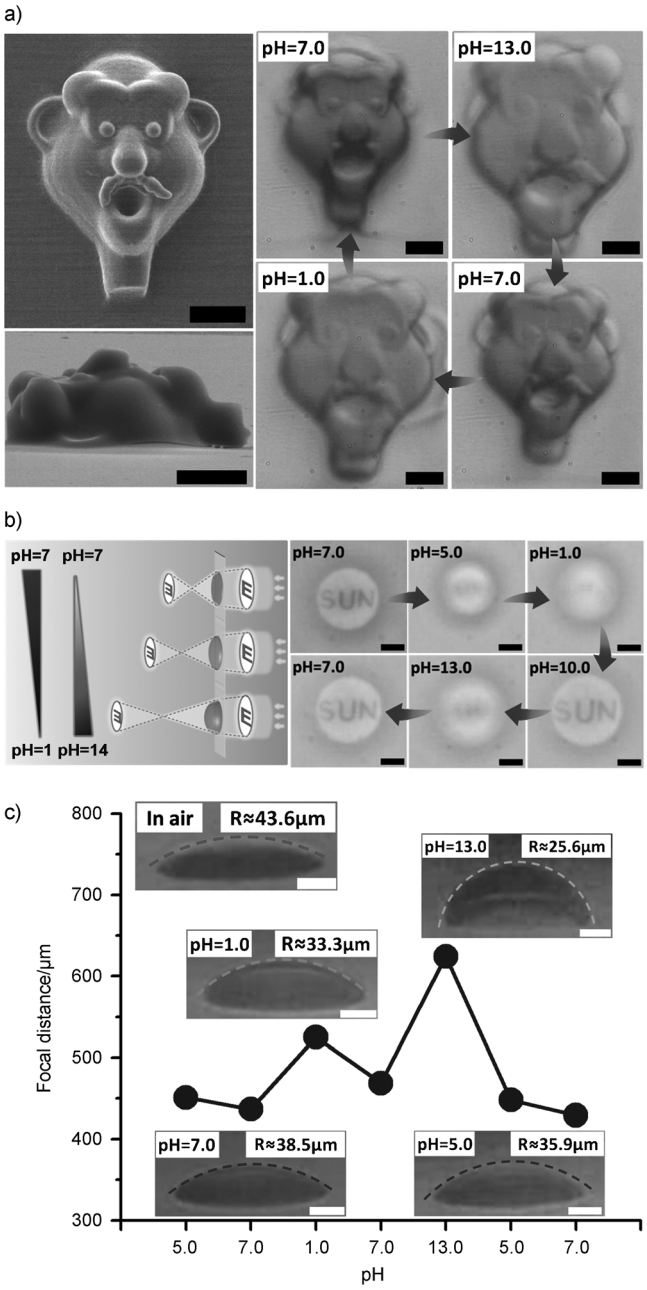

Figure 3. a) Vertical and lateral SEM pictures of a 3D relief of a face (left) and reversible deformation of the microstructure induced by changing the pH value (right). Scale bar: 10 μm. b) The effect of changing the pH value on the focusing and imaging of a protein microlens. Scale bar: 10 μm. c) Focal distance versus pH value of a protein microlens. Inset: SEM images of a protein microlens after changing the pH value. Note: The initial radius of the lens (fabricated at pH 7.4) is 20 μm and the height is 5 μm.

about 150% (from approximately 40 μm × 30 μm to approximately 60 μm × 50 μm) within seconds when the pH value was increased from pH 7 to pH 13. The structure then shrank back to the original size after the pH value was decreased to pH 7. The rapid swelling or shrinking occurs when the solvent diffuses into or out of the polymer network. In general, as the diffusion time of solvent molecules scales with the diffusion length L of polymer as L^2, microminiaturization of the protein devices helps to achieve a high response speed (less than one second).[17,25] As shown in Figure 3a, the size of the face started to swell when the pH value decreased to a lower value of pH 1. Such a pH-mediated, reversible swelling-to-shrinking cycle of the protein microstructure could be conducted many times until the elasticity was lost.

Spherical protein microlenses with diameters of 20 μm, 30 μm, and 40 μm and a height of 5 μm were fabricated (Figure 4a). Moreover, satisfactory microlenses with diameters from approximately 1 μm to about 100 μm were easily obtained. The SEM images (Figure 4a) show that these

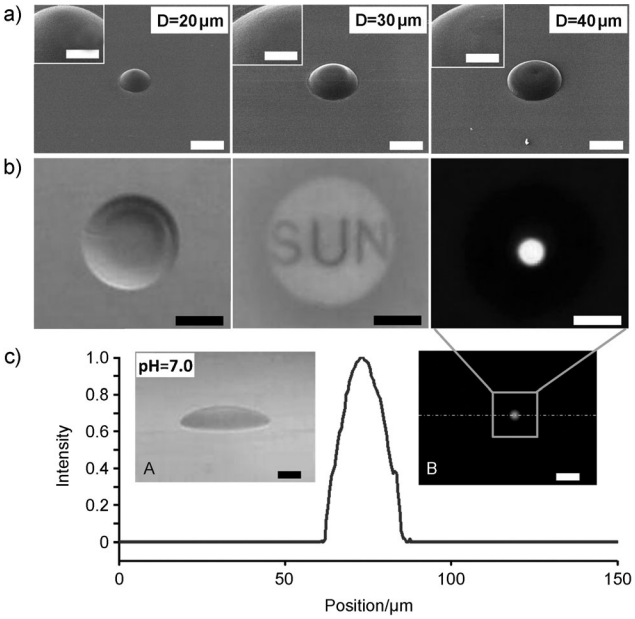

Figure 4. a) Protein microlenses with diameters of 20 μm, 30 μm, and 40 μm, respectively, and a height of 5 μm. Scale bar: 20 μm. Inset: partially enlarged details of protein microlenses with excellent surface quality. Scale bar: 5 μm. b) A protein microlens with a radius of 20 μm and a height of 5 μm (left), imaging test (center), and focusing test (right) in buffer (pH 7.0). Scale bar: 20 μm. Scale bar: 10 μm. c) Normalized intensity distribution on different positions along the line across the center of the protein microlens, which quantitatively shows the focusing ability of the lens. The FWHM of the curve is about 15 μm. Inset A: the oblique view of a protein microlens at pH 7.0. Inset B: the corresponding focusing picture.

microlenses have rather smooth surfaces. The average roughness of the lenses is about 5 nm, as shown by AFM measurements (see the Supporting Information). The optical properties of the microlenses were investigated by optical microscopy. The imaging and focusing features of the microlenses were evaluated in a phosphate-buffered saline (PBS) solution at pH 7.0. A microlens with a radius of 20 μm was used for these experiments. The optical imaging and focusing tests in the buffer are shown in Figure 4b, and demonstrate the fine shape control and optical properties of the microlens. By processing the focusing picture of the microlens and calculating the normalized intensity distribution along the dotted line, the full width at half maximum (FWHM, an expression of lens

efficiency) of the curve is about 15 μm. This value indicates that the microlens has an excellent lens efficiency (Figure 4).

Once the microlens was immersed into a solution with either a high or low pH value, the microlens started to swell (Figure 3b and c). As a consequence of restricting the lens with a glass substrate, the extent of hydrogel expansion in the horizontal direction was highly restricted so that the expansion along lateral direction was more pronounced. The changes in pH value resulted in a decrease in the curvature radius R depicted in Figure 3c. The inset pictures in Figure 3c show that the deformed microlens still has a smooth surface, as well as good lens performance. The imaging and focusing features of the lens during the tuning process were characterized by optical microscopy (Figure 3b). When the pH value was decreased from pH 7.0 to pH 1.0, the clear image became out of focus. The clear image was restored when the pH value was increased to pH 10.0. The image was then completely obscured when the pH value was increased to pH 13.0. However, the clear image was again restored when the pH value was reduced to pH 7.0. During the tuning process, we found that the microlens could withstand strong acid (pH 1.0) or strong alkali (pH 13.0). As shown in Figure 3c, the microlens can be continuously and dynamically tuned from pH 1.0 to pH 13.0. This unique feature can be used to measure the changes in pH value (1.5–9.2) in biological environments (see Table S1 in the Supporting Information). Additionally, a control experiment was carried out with a polymeric photoresist (SU-8) microlens with the same shape (see Figure S3 in the Supporting Information). However, there was no visible response upon changing the pH value.

In general, the focal length f is an important parameter for microlenses. It is well-known that a decrease in R results in a reduced f. However, in this study we found that f of a microlens (diameter = 40 μm, height = 5 μm) increased from approximately 400 μm (R = 38.5 μm, pH 7.0) to approximately 500 μm (R = 33.3 μm, pH 1.0) or even approximately 600 μm (R = 25.6 μm, pH 13.0) with a refractive index change of about 4% (Figure 3c; see also Table S2 in the Supporting Information). Normally, when the microlens is immersed in buffer, f can be calculated by $f = n_{buffer}/[(n_{hydrogel}-n_{buffer})/R + (n_{glass}-n_{hydrogel})/R']$. The notation R and R' represent two different curvature radii of the microlens, and $n_{hydrogel}$, n_{buffer}, and n_{glass} represent the refractive indices of protein hydrogel, buffer, and glass, respectively. As $R' = \infty$, the formula can be rewritten as $f = n_{buffer}R/(n_{hydrogel}-n_{buffer})$. Because the ionic strength of the buffers was fixed at 10 mM, n_{buffer} was almost constant (approximately 1.33), which was confirmed by measurement with an Abbe refractometer. Therefore, $f \approx R/(n_{hydrogel}-n_{buffer})$. Thus, the reason why f increases with the decrease in R is mainly because of the change in $n_{hydrogel}$ (see Table S2 in the Supporting Information).

The biocompatibility of the microlenses was studied in experiments with cells in vitro. Fresh rabbit blood cells were cultured together with the protein microdevices at 25 °C or at rabbit body temperature (40 °C). After co-culturing for 1 h or 24 h, the protein microdevices were transferred to physiological saline and then characterized by optical microscopy. As shown in Figure 5, red blood cells did not adhere to the microdevice surface. Similar results were also obtained in long-term cultures (several days). The surface morphology, shape, and size of microlenses did not change during the cell culture process (Figure 5), which revealed that there was no biofouling effect for this type of microlens. As a result of the excellent biocompatibility and lack of biofouling, the microlenses performed well when they were immersed into a mixture of rabbit serum and red blood cells (Figure 5c). Furthermore, their excellent optical properties were also maintained at 40 °C in the same mixture of cells (Figure 5d).

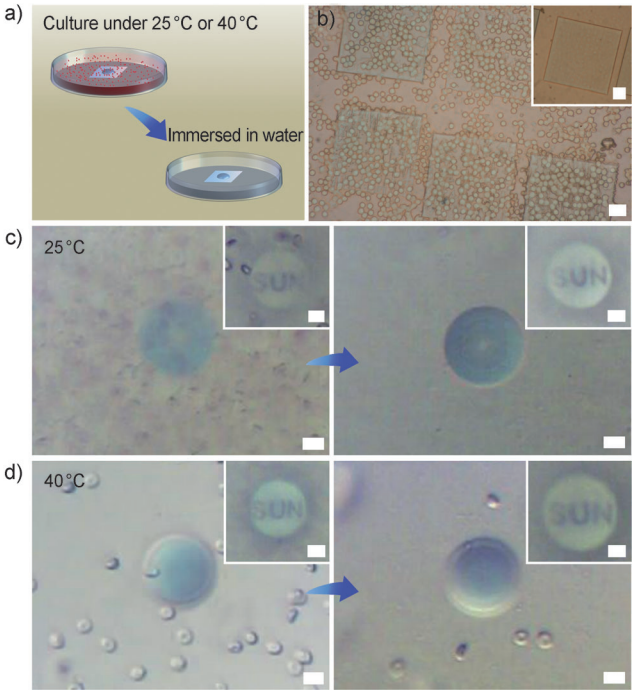

Figure 5. The biocompatibility of protein microlenses. a) In vitro cell studies. b) Optical image of protein microstructures during co-culturing with 2% rabbit red blood cell solution for 1 hour at 25 °C. Inset: after transferring to physiological saline. Scale bar: 20 μm. c) Left: the optical properties of a protein microlens in the mixture solution of rabbit serum and rabbit red blood cells at 25 °C. Right: after transferring into physiological saline. Scale bar: 10 μm. d) The optical properties of a protein microlens at 40 °C under the same experimental conditions as (c). Scale bar: 10 μm.

In summary, protein microlenses have been fabricated from BSA by maskless femtosecond laser direct writing. The photo-cross-linked protein microstructures exhibited rapid and reversible swelling-to-shrinking behavior when stimulated by chemical signals. As a result, the focal distance of the as-formed microlenses can be tuned regularly and reversibly by changing the pH value. Because of their dynamically adjustable properties and full biocompatibility, microlenses show great promise for optical, electronic, and biomedical applications. These devices may enable a new concept of protein-based photonics to revolutionize the next generation of polymeric and organic-based devices.

Received: August 22, 2011
Revised: October 19, 2011
Published online: December 12, 2011

Keywords: hydrogels · microlenses · nanotechnology · protein microdevices · synthetic methods

[1] A. Lewis, Y. Albeck, Z. Lange, J. Benchowski, G. Weizman, *Science* **1997**, *275*, 1462.
[2] A. Rizzo, N. Solin, L. J. Lindgren, M. R. Andersson, O. Inganas, *Nano Lett.* **2010**, *10*, 2225.
[3] S. T. Parker, P. Domachuk, J. Amsden, J. Bressner, J. A. Lewis, D. L. Kaplan, F. G. Omenetto, *Adv. Mater.* **2009**, *21*, 2411.
[4] R. Capelli, J. J. Amsden, G. Generali, S. Toffanin, V. Benfenati, M. Muccini, D. L. Kaplan, F. G. Omenetto, R. Zamboni, *Org. Electron.* **2011**, *12*, 1146.
[5] Z. Chen, D. Govender, R. Gross, R. Birge, *BioSystems* **1995**, *35*, 145.
[6] J. P. Mondia, J. J. Amsden, D. Lin, L. D. Negro, D. L. Kaplan, F. G. Omenetto, *Adv. Mater.* **2010**, *22*, 4596.
[7] T. Miyasaka, K. Koyama, I. Itoh, *Science* **1992**, *255*, 342.
[8] J. J. Amsden, P. Domachuk, A. Gopinath, R. D. White, L. D. Negro, D. L. Kaplan, F. G. Omenetto, *Adv. Mater.* **2010**, *22*, 1.
[9] B. D. Lawrence, J. K. Marchant, M. A. Pindrus, F. G. Omenetto, D. L. Kaplan, *Biomaterials* **2009**, *30*, 1299.
[10] V. Dinca, E. Kasotakis, J. Catherine, A. Mourka, A. Ranella, A. Ovsianikov, B. N. Chichkov, M. Farsari, A. Mitraki, C. Fotakis, *Nano Lett.* **2008**, *8*, 538.
[11] B. D. Lawrence, M. Cronin-Golomb, I. Georgakoudi, D. L. Kaplan, F. G. Omenetto, *Biomacromolecules* **2008**, *9*, 1214.
[12] F. G. Omenetto, D. L. Kaplan, *Nat. Photonics* **2008**, *2*, 641.
[13] J. Aizenberg, A. Tkachenko, S. Weiner, L. Addadi, G. Hendler, *Nature* **2001**, *412*, 819.
[14] L. P. Lee, R. Szema, *Science* **2005**, *310*, 1148.
[15] L. Dong, A. K. Agarwal, D. J. Beebe, H. Jiang, *Nature* **2006**, *442*, 551.
[16] Y. L. Zhang, Q. D. Chen, H. Xia, H. B. Sun, *Nano Today* **2010**, *5*, 435.
[17] B. Kaehr, J. B. Shear, *Proc. Natl. Acad. Sci. USA* **2008**, *105*, 8850.
[18] E. N. Frankel, W. E. Neff, T. R. Bessler, *Lipids* **1979**, *14*, 961.
[19] I. E. Kochevar, M. C. Lynch, S. G. Zhuang, C. R. Lambert, *Photochem. Photobiol.* **2000**, *72*, 548.
[20] H. R. Shen, J. D. Spikes, C. J. Smith, J. Kopecek, *J. Photochem. Photobiol. A* **2000**, *130*, 1.
[21] Q. D. Chen, D. Wu, L. G. Niu, J. Wang, X. F. Lin, H. Xia, H. B. Sun, *Appl. Phys. Lett.* **2007**, *91*, 171105.
[22] D. Wu, L. G. Niu, Q. D. Chen, R. Wang, H. B. Sun, *Opt. Lett.* **2008**, *33*, 2913.
[23] D. Wu, S. Z. Wu, L. G. Niu, Q. D. Chen, R. Wang, J. F. Song, H. H. Fang, H. B. Sun, *Appl. Phys. Lett.* **2010**, *97*, 031109.
[24] K. Takada, H. B. Sun, S. Kawata, *Appl. Phys. Lett.* **2005**, *86*, 071122.
[25] D. J. Beebe, J. S. Moore, J. M. Bauer, Q. Yu, R. H. Liu, C. Devadoss, B.-H. Jo, *Nature* **2000**, *404*, 588.

